

See discussions, stats, and author profiles for this publication at: <https://www.researchgate.net/publication/5358312>

Structure and Mutagenic Conversion of E 1 Dehydrase: At the Crossroads of Dehydration, Amino Transfer, and Epimerization †‡

ARTICLE *in* BIOCHEMISTRY · JULY 2008

Impact Factor: 3.02 · DOI: 10.1021/bi702449p · Source: PubMed

CITATIONS

9

READS

26

5 AUTHORS, INCLUDING:



Cynthia Bui

Brookdale University Hospital

1 PUBLICATION 9 CITATIONS

[SEE PROFILE](#)



NIH Public Access

Author Manuscript

Biochemistry. Author manuscript; available in PMC 2009 November 25.

Published in final edited form as:
Biochemistry. 2008 June 17; 47(24): 6329–6341. doi:10.1021/bi702449p.

Structure and Mutagenic Conversion of E₁ Dehydrase: at the Crossroads of Dehydration, Aminotransfer and Racemization,^{†,‡}

Peter Smith[§], Ping-Hui Szu[⊥], Cynthia Bui[#], Hung-wen Liu[⊥], and Shiou-Chuan Tsai^{#,§,*}

[#] Department of Molecular Biology and Biochemistry, University of California, Irvine

[§] Department of Chemistry, University of California, Irvine

[⊥] Division of Medicinal Chemistry, College of Pharmacy, Department of Chemistry and Biochemistry, University of Texas, Austin

Abstract

Pyridoxal 5'-phosphate (PLP) and pyridoxamine 5'-phosphate (PMP) are highly versatile coenzymes whose importance is well recognized. The capability of PLP/PMP-dependent enzymes to catalyze a diverse array of chemical reactions is attributed to fine-tuning of the cofactor-substrate interactions in the active site. CDP-6-deoxy-L-*threo*-D-glycero-4-hexulose-3-dehydrase (E₁), along with its reductase (E₃), catalyzes the C-3 deoxygenation of CDP-4-keto-6-deoxy-D-glucose to form the dehydrated product, CDP-4-keto-3,6-dideoxy-D-glucose, in the arscarylose biosynthetic pathway. This product is the progenitor to most 3,6-dideoxyhexoses, which are the major antigenic determinants of many Gram negative pathogens. The dimeric [2Fe-2S]-protein, E₁, cloned from *Yersinia pseudotuberculosis*, is the only known enzyme whose catalysis involves the direct participation of PMP in one-electron redox chemistry. E₁ also contains an unusual [2Fe-2S] cluster with a previously unknown binding motif (C-X₅₇-C-X₁-C-X₇-C). Herein we report the first X-ray crystal structure of E₁, which exhibits an aspartate aminotransferase (AAT) fold. A comparison of the E₁ active site architecture with homologous structures uncovers residues critical for the dehydration versus transamination activity. Site-directed mutagenesis of four E₁ residues – D194H, Y217H, H220K, and F345H – converted E₁ from a PMP-dependent dehydrase to a PLP/glutamate-dependent aminotransferase. The E₁ quadruple mutant, having been conferred this altered enzyme activity, can transaminate the natural substrate to CDP-4,6-dideoxy-4-amino-D-galactose without E₃. Taken together, these results provide the molecular basis of the functional switch of E₁ towards dehydration, epimerization, and transamination. The insights gained from these studies can be used for the development of inhibitors of disease-relevant PLP-PMP-dependent enzymes.

Vitamin B₆ derived pyridoxal 5'-phosphate (PLP) and pyridoxamine 5'-phosphate (PMP) are coenzymes with extraordinary catalytic versatility (1). PLP/PMP-containing enzymes catalyze diverse chemical reactions such as transamination, dehydration, racemization, decarboxylation, and β-,γ-elimination/substitution. The catalytic versatility of this class of enzymes is largely controlled by the specific coenzyme-substrate interactions in the active-site, where the chemical properties of the coenzyme, modulated by the surrounding residues, determine the outcomes of the reactions (2). Because PLP/PMP-containing enzymes often play critical roles in pathogenesis and metabolism, they have been targeted for potential therapeutics to treat conditions such as cancer (3), infectious diseases (4) and Parkinson's disease (5).

[†]This work was supported by NIH Grant GM35906 to H.-w. L and the Pew Foundation to S.-C. Tsai.

[‡]Coordinates and observed structure factor amplitudes have been deposited in the Protein Data Bank (PDB codes 3BCX and 3BB8)

*Corresponding address: Department of Molecular Biology and Biochemistry, Department of Chemistry, University of California, Irvine – 2302 Natural Science I, Irvine, CA 92697. Phone (949) 824-4486; fax (949)824-8552; sctsai@uci.edu.

Because the success of drug development commonly relies on exploiting the catalytic properties of the target enzymes, such that the drug inhibits only the intended target, understanding the molecular basis of reactions catalyzed by PLP/PMP-dependent enzymes is not only of scientific interest, but may also produce new therapeutic agents.

The 3,6-dideoxyhexoses, found predominantly in the *O*-antigen of lipopolysaccharides (LPS) (6), have been shown to be the major antigenic determinants of the Gram-negative bacteria (7). In Nature, CDP-6-deoxy-L-*threo*-D-glycero-4-hexulose-3-dehydrase (E_1), along with its reductase (E_3), catalyzes the C-3 deoxygenation of CDP-4-keto-6-deoxy-D-glucose (1) in the presence of NADH to form CDP-4-keto-3,6-dideoxy-D-glucose (2) in the 3,6-dideoxyhexose biosynthetic pathway (Fig. 1–2) (8). Product 2 is the common precursor to at least four of the seven naturally occurring 3,6-dideoxyhexoses, namely abequose, ascarylose, paratose, and tyvelose (Fig. 2) (8). The importance of 3,6-dideoxyhexoses to Gram-negative pathogenicity makes E_1 an appealing target for inhibitors that could attenuate the effects of this Gram-negative bacterial arsenal. Crystal structures of E_1 will facilitate the development of E_1 -inhibiting molecules.

E_1 is homologous to proteins in the PLP-containing aspartate aminotransferase (AAT) superfamily (9). Many of them serve as dehydrases or aminotransferases in nucleotide sugar biosynthetic pathways (10–13). Interestingly, E_1 contains a [2Fe-2S] cluster in addition to PMP (14), distinguishing E_1 from these other enzymes. This unusual structural feature is even more intriguing, because the cysteine ligands of the iron-sulfur cluster have a C-X₅₇-C-X₁-C-X₇-C motif, which is unique among [2Fe-2S]-containing enzymes (15). Determination of the crystal structure of E_1 can help verify the configuration of this unique [2Fe-2S] cluster and provide a structural basis to elucidate the PMP-radical mechanism distinctly observed in E_1 .

In this work, we present the first crystal structures of the wild type E_1 , the PLP-bound H220K- E_1 mutant protein, and a sugar substrate-bound H220K- E_1 . Previously, H220 was proposed to be an important catalytic residue (16). Because of nearly invariable sequence overlap of a lysine in this position across homologous aminotransferases, the H220K mutation was generated to determine if this singular alteration could convert E_1 from a dehydrase to an aminotransferase (17). Indeed, the H220K mutation changed E_1 from a PMP-dependent dehydrase to a PLP-dependent, non-catalytic aminotransferase. (17) However, the molecular nature that distinguishes a dehydrase versus an aminotransferase is not clear, and additional E_1 residues need to be mutated to generate a catalytic aminotransferase. The wild type and H220K E_1 crystal structures provide molecular resolution of the catalytic residues involved, and shed light on factors governing substrate specificity. Moreover, the crystal structures identify a histidine (H278) instead of a cysteine (C192 or C193) residue as the fourth ligand of the unique [2Fe-2S] motif in E_1 . This information offers considerable insight into the catalytic mechanism of E_1 , and enables a critical evaluation of the differences between a dehydrase and a transaminase in vitamin B₆-dependent enzymes. On the basis of these structures, mutagenesis of four active-site residues successfully transformed E_1 from a PMP-mediated C-3 dehydrase into a PLP/L-glutamate-dependent C4 aminotransferase (Fig. 2). Together, these results provide a structural rationale for the chemistry carried out by the E_1 - E_3 complex, and lay the foundation for future development of inhibitors able to attenuate infectivity of Gram-negative pathogens.

MATERIALS AND METHODS

Chemicals and DNA Manipulation

All chemicals were purchased from Sigma-Aldrich Chemical Co. and were the highest grade available. The H220K mutation (pTrc99A) was generated previously (17). The quadruple mutants were constructed in three PCR rounds by using the Quik-Change Site-Directed Mutagenesis kit (Stratagene). Synthetic oligonucleotides were from Operon. The following

primers, from 5'-3', were used for mutagenesis: D194H - GAAGACTGCTGCCATGCGTGGTTCC, Y217H - GGTACCGTTAGCTTCCATCCCGCTAACATATC, F345H - GATCCATCATGGCATGGTTCCCTATCACTCTG. Reverse primers were inverse complements of the forward primers. Point mutations were confirmed by sequence analysis. Strain BL21 λ(DE3) was used for recombinant protein expression.

Protein Expression and Purification

The wild type and H220K mutant of E₁ follow the same procedure as described previously (17,18). Unlike the wild type and H220K variants of E₁, the E₁ 4x mutant purification was carried out aerobically on the basis of the proposed mechanism where the iron-sulfur cluster was not of concern for the speculated chemistry, though 5 mM DTT was included in all buffers. Recombinant E₁ 4x mutant was expressed in *E. coli*. Cultures were grown in LB broth with 100 mg/L ampicillin. At OD₆₀₀=0.6–0.8, protein expression was induced by 0.1 mM isopropyl β-D-thiogalactoside (IPTG) and the cultures were grown at 18 °C overnight. Cells were harvested by centrifugation (5,000 × g for 20 min), followed by resuspension, sonication, and centrifugation for cell debris removal (18,000 × g for 1 hr). The lysis buffer was 50 mM Tris-HCl, pH 7.5 (buffer A). The solution was loaded onto DEAE sepharose media pre-equilibrated with buffer A. After washing with buffer A, a linear gradient of NaCl from 0 to 500 mM in buffer A was run with a gradient-maker via gravity. Brown fractions were collected and dialyzed in 4 L buffer A overnight. The sample was concentrated and passed over a Mono Q 5/50 GL column. A linear gradient from 0 – 100% buffer B (buffer A made 0.5 M in NaCl) was run over 20 column volumes. The A₂₈₀ displayed multiple overlaid peaks in the region of the suspected protein. SDS-PAGE confirmed the inclusion of multiple proteins in the sample.

Crystallization, Data Collection

Crystals for the wild type and H220K mutant E₁ were grown in anaerobic and aerobic environments, respectively, at 2 mg/mL in 0.1 M HEPES (pH 7.6), 1.0 M ammonium sulfate, 2% (v/v) PEG 400, and 2% (v/v) benzamidine hydrochloride by the sitting drop vapor diffusion method at 25 °C. Substrate-bound crystals of the H220K mutant E₁ were grown as the H220K mutant E₁ with the exception that the protein sample was mixed with 1 mM (50-fold molar excess) of synthetically made CDP-4,6-dideoxy-4-aminoglucose **9** (7), and left to incubate on ice for 1 hr prior to adding the sample to the crystal tray. Prior to diffraction, crystals were cryoprotected in 2 M lithium sulfate and frozen in liquid N₂. Diffraction data were collected at the Stanford Synchrotron Radiation Laboratory (SSRL) and Advanced Light Source (ALS), and integrated and reduced using HKL2000 (20) (Table 1).

Molecular Replacement and Refinement

The wild type E₁ crystal structure was determined by molecular replacement in CNS, using the crystal structure of AHBA synthase as the search model (13,21). After rebuilding with Quanta, further refinement was performed in CNS using torsion angle simulated annealing followed by energy minimization, and positional and individual B-factor refinement. Subsequent rounds of model building and refinement were carried out with the maximum likelihood approach implemented within CNS. Water molecules were added and edited both visually and with an automated water picking program (CNS) to afford an R_{crys} of 20.8 % (R_{free} =23.1 %), (Table 1) (21). The H220K E₁ and the substrate-bound H220K E₁ structures were solved via molecular replacement using the wild type structure as the search model, and refined by CNS to afford an R_{crys} of 21.9 % (R_{free} =25.0 %), and 21.5 and (R_{free} =25.9 %), respectively (Table 1).

Location of Singular Iron Site on Wild-type E₁ Structure

Upon synchrotron irradiation of the crystal (back-soaked in iron-free cryoprotectant prior to freezing) at the iron-absorption edge, a strong fluorescence signal was detected, indicating the presence of iron in the crystal. However, the disordered nature of the iron-binding E₁ loop precludes the precise location of the iron site. However, large anomalous peaks were observed from the anomalous difference map (FT (fom ($|f_a+|-|f_a-|$) $\exp(i[\text{phase}-90])$) calculated by CNS, using the experimentally determined peak wavelength (1.73970 Å) of the 3-wavelength dataset (Table S1). The phase includes the model phase calculated from refined E₁ model. A simulated annealing composite omit map was subsequently generated by CNS that corroborated the peak from the anomalous FT map with a defined patch of electron density outside the current protein model, and overlaying perfectly on the highest anomalous difference peak (5.62 I/sigma) that is located near the end of the disordered loop, where iron is expected to bind E₁.

Quantitation of Enzyme-Bound Iron in Wild-type, H278A, and H278C Mutants

The enzyme-bound iron was determined by a literature procedure (19). The standard curve was determined using Fe(NH₄)₂(SO₄)₂. Protein samples (1 mL each) for iron titration analysis were mixed with 500 μL of reagent A (1:1 of 4.5% KMnO₄:1.2 N HCl) and incubated at 60°C for 2 h. To these samples were added 100 μL of reagent B (8.8 g of ascorbic acid, 9.7 g of ammonium acetate, 80 mg of ferrozine, 80 mg of neocuproine, and ddH₂O to 25 mL total volume) followed by immediate vortexing. The absorbance of the samples was determined at 562 nm after the samples had incubated for 1 h at room temperature. Purified E₁ contained approximately 1.95 iron per monomer, consistent with E₁ containing a [2Fe-2S].

The Activity Assay of H278A and H278C Mutants

The activity of wild-type, H278A, and H278C E₁ was determined by a previous published procedure (16). Briefly, the activity was determined by an assay coupling E₁ with E₃. The assay mixture consists of 25 μM PMP, 200 μM NADH, 100 μM CDP-4-keto-6-deoxy-D-glucose (**1**) and an appropriate amount of E₃ in 800 μL of 50 mM potassium phosphate buffer (pH 7.5). The reaction was initiated by the addition of E₁, and the E₁ activity was determined by measuring the rate of decrease of the absorbance at 340 nm ($\epsilon_{340} = 6220 \text{ M}^{-1} \text{ cm}^{-1}$) within the initial 1 min. Each reading was calibrated against background activity (about 2% corresponding to the E₃-catalyzed oxidation of NADH in the presence of O₂) which was recorded prior to the addition of E₁. The E₁-induced NADH oxidation which was measured individually was also subtracted from the observed readings. The specific activity of wild-type E₁ was 85 U/mg of protein, which was comparable to those previously reported.

The PLP Reconstitution of the E₁ Quadruple Mutant

The purified E₁ quadruple mutant was reconstituted with ten-fold excess of PLP at 4 °C for 1 h and subsequently dialyzed against 50 mM potassium phosphate buffer (pH 7.5) with four times of buffer change. The reconstituted protein was concentrated by ultrafiltration through YM10 Diaflo membrane (Amicon).

The Activity Assay of the E₁ Quadruple Mutant

Activity assays were carried out in 50 mM potassium phosphate buffer, pH 7.5 in the presence of 1 mM substrate (CDP-4-keto-6-deoxy-D-glucose, **1**), 50 μM E₁ quadruple mutant, 1.5 mM PLP, and 4.5 mM L-glutamate. The final volume of the assay mixture was 0.5 mL. The reaction mixture was incubated at 25 °C and the reaction was then stopped at different time points by removing the enzymes by filtration through YM10 Diaflo membrane (Amicon). The reaction progress was monitored by HPLC on a CarboPac PA1 anion exchange column (4 × 250 mm) obtained from Dionex (Sunnyvale, CA). The flow rate was 1.0 mL/min and the detector was

set at 267 nm. A linear gradient from 2.5% to 10% buffer B (1 M ammonium acetate, pH 7.0) in buffer A (ddH₂O) over 20 min, followed by a second linear gradient from 10% to 30% buffer B in buffer A over 20 min gave a satisfactory separation between substrate **1** and the new product (at around the retention time 10 min). The new product was collected and subjected to mass spectrometry analysis. The new product was identified as CDP-4,6-dideoxy-4-aminogalactose **12** on the basis of its retention time, which was identical to that of a chemically synthesized standard (17), as well as high-resolution ESI-MS data (calcd for [M·H]⁺: 547.0843, found: 547.0841). The maximum percent conversion was 32% after incubation at 25 °C for 27 h. The small bump eluted at around 25 min in HPLC trace is a decomposition product, CMP, derived from the substrate during HPLC analysis.

Steady State Kinetics of the E₁ Quadruple Mutant

The First Half-reaction—The E₁ quadruple mutant was reconstituted with 10-fold excess of PLP by incubating the enzyme and PLP at 4 °C for 1 hr. Subsequently, the excess amount of PLP was removed by dialysis against 50 mM KPi buffer (pH 7.5) containing 1 mM DTT with three times of buffer change. The reaction mixture contained 25 μM of reconstituted enzyme and 20 mM of L-Glu in 50 mM KPi buffer (pH 7.5) containing 1 mM DTT. The total reaction volume was 250 μL and the reaction mixture was incubated at 25 °C. Reaction progress was followed by monitoring the absorbance maxima of the PMP and PLP cofactor forms at 340 nm and 430 nm, respectively. Resulting time courses were fit to the equation: $y = A(1 - \exp(-kt)) + C$

y = observed signal; k = the apparent first order rate constant; t = time.

The Second Half-reaction—The E₁ quadruple mutant was reconstituted with 10-fold excess of PMP by incubating the enzyme and PMP at 4 °C for 1 hr. Subsequently, the excess amount of PMP was removed by dialysis against 50 mM KPi buffer (pH 7.5) containing 1 mM DTT with three times of buffer change. The reaction mixture contained 25 μM of reconstituted enzyme and 270 μM of sugar substrate **1** in 50 mM KPi buffer (pH 7.5) containing 1 mM DTT. The total reaction volume was 250 μL and the reaction mixture was incubated at 25 °C. Reaction progress was followed by monitoring the increase of the absorbance at 430 nm (the PLP cofactor form). Resulting time courses were fit to the equation: $y = A(1 - \exp(-kt)) + C$

y = observed signal; k = the apparent first order rate constant; t = time.

The activity data are summarized in Table 2.

RESULTS AND DISCUSSION

Overall Fold

Similar to the seven homologous enzymes (13,22–27), E₁ and the H220K mutant have folds typical of the AAT superfamily. When the Fe-S-coordinating loop is excluded, the wild type and H220K E₁ structures can be superimposed with RMSD of 1.23–1.4 Å. However, the wild type structure does not contain the cofactor, while the cofactor PMP is clearly present in the H220K structure. For this reason, we display the H220K structure in Fig. 3 instead of the wild type structure (2). Both the wild type and the H220K-E₁ exist as dimers in the crystal form, similar to results obtained in solution and reported previously (Fig. 3A). In both structures, the two monomers are nearly identical, with an RMSD < 0.25 Å. E₁ has a conserved N-terminal large cofactor binding domain and a C-terminal small domain (Fig. 3B). The N-terminal helices (A, B, C) precede the large domain, which has a central seven stranded β-sheet (strand order 1-7-6-5-4-2-3) with strand 7 anti-parallel to the remaining strands. The central β-sheet is surrounded by three α-helices (C, G, F) opposite to the active site opening, along with four α-

helices (H, D, E, K) facing the active-site pocket opening; the macrodipole of helix D may play a role in stabilizing the phosphate moiety of the cofactor. After the large cofactor domain is a Fe-S-coordinating loop (residues 249–280, with 253–268 disordered), which then leads into the C-terminal domain consisting of four helices (I, J, K, L) and strands 8–10. Clearly, E₁ has all the hallmark structural features of the AAT superfamily, though distinguishes itself from this enzyme family with the presence of the unique Fe-S-coordinating loop (10,11,28).

The Cofactor Binding Site

The wild type active pocket, though lacking the PMP cofactor, exhibits a PMP-binding architecture similar to PMP-bound homologous structures, such as BtrR (23), ArnB (25) and PseC (27). The residues defining the PLP/PMP binding motif, including S86, G87, S88, F120, T122–123, D191, S215, E226, G227, W247, R264, N288, and F377 are highly conserved (Fig. 5). These residues in the apo wild-type E₁ and PLP-H220K-E₁ structures are almost superimposable (Fig. 4A). The PLP-H220K-E₁ structure shows well defined PLP electron density as a covalent Schiff base adduct between the amino group of K220 and the C4' carbonyl group of PLP (internal aldimine, Fig. 4B). The lysine aldimine group is 35 degrees out of plane of the PLP pyridine ring, and 2.75 Å away from the 3' oxygen of the ring (salt bridge), (Fig. 4C). This PLP-enzyme binding motif is consistent with homologous PLP-containing enzyme structures (13,22–27). Therefore, although the wild type structure of E₁ was solved without well defined electron density of the natural cofactor PMP, the PMP docking position in the wild type enzyme is expected to mirror the PLP position in H220K-E₁.

Similar to homologous enzyme structures, the E₁ active site is composed of residues from both monomers (Fig. 4A–C) (9). In the PMP/PLP binding pocket, the conserved W247 from one monomer aids in stabilizing the PLP phosphate of the opposite monomer via side chain hydrogen bonding. In addition, the G86 backbone nitrogen, S87 side chain and backbone nitrogen, and the S215 side chain all directly hydrogen bond with the PMP/PLP phosphate, while the E226 side chain and G227 backbone indirectly help stabilize the same phosphate via an ordered water (Fig. 4C). The α-helix D macrodipole also helps stabilize the anionic cofactor phosphate. The highly conserved D191 forms a salt bridge with the pyridinium nitrogen of PLP stabilizing the protonated state of the cofactor, a key to the “electron sink” property of PLP/PMP (Fig. 4C) (1, 2). It is intriguing that E₁ has such unique catalytic capacities considering that residues important for cofactor bindings are highly conserved between E₁ and homologous PLP/PMP enzymes (Fig. 5).

The Substrate Binding Pocket

Compared to the highly conserved PLP/PMP pocket in E₁, the putative sugar substrate binding site is less conserved. Despite repetitive efforts to collect diffraction data from E₁-PLP-sugar co-crystals, we could not obtain the full occupancy of the aminosugar (CDP-4,6-dideoxy-4-amino-D-glucose **8**). However, the Fo-Fc omit map (contoured at 3.0 sigma) of aminosugar-bound structure has well defined density of PLP, as well as partial electron density of the CDP-sugar moiety. This positions the aminosugar in between the electron density of PLP and CDP, and the sugar location is highly consistent with docking simulation of the aminosugar **8** into the H220K mutant structure. In 20–30 independent rounds of sugar-E₁ docking simulations (with no bias), we consistently identify a docking mode that extends from the cofactor C4' nitrogen towards the enzyme surface (Fig. 6D). This docking mode overlaps consistently with the above broken electron density observed in the H220K E₁-PLP-sugar co-crystal data (Fig. 6A, B, E). On the basis of the docking results and partial electron density of PLP-sugar, we can identify residues proximal to the sugar substrate. Sequence alignment with the homologous enzymes revealed that these sugar binding residues are only partially conserved (Figs. 5, 6F). Specifically, the ribose-interacting residues K39-Y217-P218 of monomer A are not conserved, and the diphosphate-interacting residues such as S37-R374 of monomer A and K279-Y280 of

monomer B are semi-conserved, especially K279-Y280. Because E₁ is the only CDP-sugar binding enzyme among the homologous structures, the cytidine-interacting residues such as K39 of monomer A and W57-T59 of monomer B are the least conserved residues in the pocket. That many of the sugar recognition residues are not conserved is not surprising, because these variations are necessary to permit different substrate specificities in different enzymes. Interestingly, the majority of residues interacting with the sugar moiety are semi-conserved aromatic residues, including F120-Y217 of monomer A and W247-Y280-Y282 of monomer B that interact with the sugar backbone and hydroxyl groups via hydrogen bonds (Fig. 5).

The Fe-S Coordinating Loop

E₁ exhibits a unique [2Fe-2S] coordination motif that currently has no structural precedent. These coordinating residues, identified by systematic mutations of the E₁ cysteines, indicated that C251, C253, and C261 are essential for retaining enzyme activity and preserving the [2Fe-2S] cluster (15). The residues lie on a disordered loop in both the wild type and H220K-E₁ crystal structures (residues 253 – 267, Fig. 3A–B) located at the protein surface. While no [2Fe-2S] cluster is visible in the crystal structures, the location of one iron of the iron-sulfur center can be identified from a large peak in the anomalous difference electron density map calculated from the MAD data, (Fe peak wavelength at 1.74 Å, Table S1, Fig. 7A), with a signal to noise ratio of 5.6. The anomalous iron peak lies near the 253-268 loop region.

Previous mutagenesis showed that double alanine mutations of C192 and C193 resulted in the loss of iron-binding capability, suggesting that the fourth Fe-coordinating residue is C192 or C193, and C192/C193 can substitute for one another. The positions of C192 and C193 are well defined in the apo and H220K-E₁ structures. However, to our surprise, these two cysteines are buried at the bottom of the E₁ active site, inaccessible to solvent or the would-be surface [2Fe-2S] cluster. Hence, neither C192 nor C193 likely plays a role in Fe coordination. A highly improbable large rearrangement of the protein structure is required (22 Å, Fig. 7C) to move C192/C193 close to the other iron ligands (C251/C253/C261). The loss of iron binding in the C192A and C193A mutants is probably a result of mutation-induced conformational change, rather than a direct loss of the iron-coordinating cysteine. Interestingly, the crystal structure of E₁ reveals that the fourth ligand is likely H278 which occupies an iron coordination site, along with the proposed C251 and C253 (Fig. 7A–B) (15). An omit map (Fo-Fc, contoured at 3.0 sigma) displays clear density for the H278 side chain, and additional, less well-defined density stretches from the proposed iron site indicates protein residues (albeit in disorder) in this region (Fig. 7A–B). To examine the role of H278, the H278A and H278C mutants were prepared. As expected, the H278A-E₁ mutant is incapable of holding iron and is catalytically inactive. In contrast, the H278C-E₁ mutant retains approximately 50% of the iron content and the catalytic activity when compared to the wild type E₁. These results further substantiate the assigned role of H278 in iron-sulfur cluster binding.

The disorder in the 253-267 loop region of E₁ is unusual among AAT enzyme structures. Except ArnB (25), which has an 11-residue gap, all other homologous enzyme structures have ordered loops in this region, including ColD (22), BtrR (23), DesV (26), PseC (27), and AHBA synthase (13). This loop region is the least conserved region between E₁ and the other six enzymes (Fig. 5). When the structure of E₁ is superimposed on the homologous structures (Fig. 7D), it becomes obvious that the 253-267 loop region of one monomer, if connected, is adjacent to the active site of the other monomer. The well-studied aspartate transaminase is active only in the open conformation (2). Hence, a possible explanation for the loop flexibility observed in E₁ is that it allows “open” and “closed” conformational changes of the substrate binding pocket as a gating mechanism. However, in the homologous ColD (22), BtrR (23), and especially PseC (27), whose apo and substrate/inhibitor-bound structures are available for comparisons, this loop region remains unchanged with and without substrate binding. These observations

suggest that a second possible reason for the E₁ loop flexibility is to allow close contact with the reductase E₃ to form a reasonably tight binary complex (29). Such a complex would facilitate electron transfer from the reduced iron-sulfur center of E₃ via the iron-sulfur cluster of E₁ to reduce the dehydration product **4** in the E₁ active-site.

The Structural Basis for the Dehydrase and Aminotransferase Activities

While the wild type E₁ is a dehydrase, many of its close homologs are aminotransferases, such as ColD (22), BtrR (23), ArnB (25), DesV (26), and PseC (27). The two most obvious distinctions between E₁ and the AAT relatives are the presence of the [2Fe-2S] cluster and the switch of the active site lysine to a histidine (H220) in E₁ (15). Prior to solving the E₁ crystal structures, in a retro-evolutionary attempt to convert E₁ from a dehydrase to an aminotransferase, we constructed the E₁ H220K mutant, and found that H220K-E₁ acts as a PLP-dependent transaminase with no dehydrase activity (17). We reasoned that the newly introduced K220 could form an external aldimine (**9**) with an incoming aminosugar substrate (**8**) (Fig. 2). The reaction proceeds via tautomerization to give **3**, which after hydrolysis produces PMP and a ketosugar product (**1**). While this single mutation altered the function of E₁, the reaction is unfortunately not catalytic since PLP cannot be regenerated after each catalytic cycle (Fig. 2, path A). With the E₁ crystal structures in hand, we can dissect the molecular features that discriminate between dehydrase and aminotransferase activities.

Among the above homologous aminotransferases, ArnB (25) works on a uridine 5'-diphosphate ketopyranose (PDB code 1MDX, 1MDO, 1MDZ, 1O61 and 1O62), which closely resembles the substrate for E₁ (Fig. 8A). For this reason, we chose ArnB as the aminotransferase model for comparison with E₁. Four putative active site residues were identified that are different between E₁ and ArnB: D194, Y217, H220, and F345 in E₁, and the corresponding H163, H185, K188, and H297 in ArnB (Fig. 5).

To examine if these four residues are important for the aminotransferase activity of ArnB, and if E₁ can be imparted this catalytic capacity, we generated the D194H-Y217H-H220K-F345H quadruple mutant, and incubated a catalytic amount of the mutant enzyme with large excess of PLP and L-glutamate in the presence of the biological substrate, CDP-4-keto-6-deoxy-D-glucose (**1**, see Fig. 8B for HPLC trace). HPLC analysis of the incubation mixture revealed the formation of a new product which was identified as CDP-4,6-dideoxy-4-amino-D-galactose (**12**), based on its retention time, which is identical to that of a standard (17), and high-resolution ESI-MS data (calculated for [M·H]⁺: 547.0843, found: 547.0841). The control experiment conducted with E₁-plasmid-free competent cells did not produce any turnover product. Thus, the quadruple mutation has successfully converted E₁ into a catalytic, PLP/L-glutamate-dependent transaminase that closely mimics the ArnB activity.

E₁ Quadruple Mutant Kinetic Efficiency

Upon determining that the E₁ quadruple mutant could produce the amino sugar, **12**, we sought to compare its kinetic efficiency relative to the ArnB aminotransferase. The two half reactions are monitored using the distinct absorbance maxima of enzyme-PMP (E-PMP) and enzyme-PLP (E-PLP) at 340 nm and 430 nm, respectively (Fig. 9). The first half reaction involves amino transfer from L-glutamic acid to the E-PLP complex to generate E-PMP and α-ketoglutarate. In the second half reaction, adding the CDP-ketosugar substrate **1** to the E-PMP results in amino transfer from the E-PMP to generate the amino sugar **12**, and regenerate E-PLP (Fig. 9). In the first half reaction, the curves fitted to the data in Fig. 9 give consistently observed rate constants of $0.0266 \pm 0.002 \text{ min}^{-1}$ and $0.0277 \pm 0.0021 \text{ min}^{-1}$ for data obtained at 340 nm and 430 nm, respectively. The observed rate constants published for ArnB aminotransferase in the first half reaction were $0.065 \pm 0.014 \text{ min}^{-1}$ and $0.051 \pm 0.013 \text{ min}^{-1}$ at 340 nm and 430 nm, respectively (25), in which the amino donor is L-methionine.

Therefore, the reported activity of ArnB aminotransferase is comparable in magnitude to the observe activity of the E₁ quadruple mutant for the first half reaction.

The second half activity of ArnB is not reported in the literature, although Breazeale et al reported the overall ArnB activity as 1.3×10^3 nmol min⁻¹mg⁻¹ for the appearance of the amino sugar product (30). Since the second half rate constant in the E₁ quadruple mutant is 10 times slower than the first half rate constant, it appears that for the E₁ quadruple mutant, the rate limiting step is in the second half reaction, which approximates the overall turnover. In the second half reaction, the E₁ quadruple mutant has a k_{obs} of 0.0035 ± 0.0001 min⁻¹, which can be converted to 9.6 nmol min⁻¹mg⁻¹ for the appearance of E-PLP, assuming E-PLP extinction coefficient is 8050 at A₄₃₀, as reported in the literature (31). Therefore, the overall rates of ArnB and the E₁ quadruple mutant are differed by two orders of magnitude, which may be caused by the nature of the protein mutations, or by the different binding ability of substrate/transition state because ArnB and E₁ have different sugar substrates (Fig. 8A), and the sugar-binding residues in ArnB and E₁ are not conserved (Fig. 5).

At the Crossroads of Transamination, Dehydration and Epimerization

The above result is distinctly different from what was observed with the single H220K mutation that allowed non-catalytic conversion of CDP-4,6-dideoxy-4-amino-D-glucose (**8**), but not CDP-4,6-dideoxy-4-amino-D-galactose (**12**), into **1** (17). Figure 2 summarizes the chemistry catalyzed by E₁ and its mutants. The wild type E₁ catalyzed reaction follows the route **1**→**3**→**10**→**4**→**6**→**2** (Fig. 2, path C), starting with the formation of a Schiff base **3** between PMP and the substrate **1**, followed by C4' deprotonation to form the quinonoid intermediate **10**, β-elimination of the 3-OH group to give **4**, and then reduction in the presence of reductase E₃ to generate **2** via **6**. The overall conversion is a PMP-dependent C-3 deoxygenation (**1**→**2**). The reaction mediated by H220K-E₁ proceeds via the route **8**→**9**→**10**→**3**→**1** (Fig. 2, path A), starting with the exchange of the internal aldimine **7** formed between PLP and K220 to the external aldimine **9** formed between PLP and the aminosugar **8**. Subsequently, deprotonation at C4 of the sugar substrate generates the quinonoid intermediate **10**. The final steps involve the reprotonation at C4' of the cofactor to generate **3**, which is then hydrolyzed to produce **1**. The overall transformation is a transamination reaction (**8**→**1**). However, the reaction is not catalytic since the coenzyme is not regenerated. In contrast, the quadruple mutant-catalyzed reaction (**1**→**12**) is fully catalytic and is initiated by the transamination of PLP and L-glutamate to produce PMP and α-ketoglutarate. The subsequent steps, following the route **1**→**3**→**10**→**11**→**12** (Fig. 1, path B), include formation of the Schiff base **3** between PMP and **1**, deprotonation at C4' of the cofactor to form the quinonoid intermediate **10**, reprotonation at C4 of the sugar substrate from the equatorial position to give the aldimine **11**, and transamination with K220 to give the product **12** and the internal aldimine **7**. It is evident that the quinonoid intermediate **10** sits at the crossroads of transamination, epimerization, tautomerization, and β-elimination, and the outcomes of the reaction depend on the regioselectivity of the protonation/deprotonation processes mediated by different active-site residues.

To identify residues responsible for protonation/deprotonation in the preceding three reaction types, we carried out extensive *in silico* docking of the coenzyme-sugar adducts **9**, **10** and **11** into the active sites of the H220K-E₁ and the quadruple mutant homology model (Fig. 10A–C). Our results show that each coenzyme-substrate adduct has a unique docking mode, and can help to explain the different chemical outcomes. Docking **9** or **10**, the best result places K220 close to the hexose C4 axial position (Fig. 10A), allowing for pathway **8**→**9**→**10**→**3**→**1**, with K220 serving as active base/acid for tautomerization. The result for adduct **11**, with either H220K-E₁ or the quadruple mutant, yielded a specific binding mode positioning K220 away from the C4 axial position (Fig. 10B). Docking of **10** into the quadruple mutant shows that

either H217 or H194 can protonate substrate **10** at the C4 equatorial position to generate **11** (Fig. 10C), leading to product **12**. H220K-E₁ cannot carry out this reaction lacking these two histidines. None of the above residues exist in the active site of the wild type E₁ to carry out C4 protonation, where dehydration (via C3-OH protonation) takes place instead, presumably activated by a water, hydrogen bonded to Y280 or Y282.

Biological Significance

The wild type and H220K-PLP E₁ crystal structures provide new insights into the architecture and chemistry employed by this dehydrase. The three-dimensional picture allows visualization of the active site, which corroborates the role of H220 as a catalytic acid/base, and identifies residues important for transamination/dehydration/epimerization. One of the unusual features of the E₁ dehydrase is the [2Fe-2S] cluster. The crystal structures have located the Fe site for the first time on the protein surface, as well as clarified residues that coordinate to the Fe. When compared with homologous structures, the E₁ structures also enable us to mutagenically convert the enzyme into a catalytic, PLP/L-glutamate dependent aminotransferase. The significance of the quadruple mutant results are twofold: the mutant identifies the four key active site residues necessary to distinguish between a dehydrase and an aminotransferase, and for the first time, it is possible to correlate mutated residues in the two different E₁ mutants (the quadruple versus H220K) with different specificities towards epimeric sugars (CDP-4,6-dideoxy-4-aminoglucose versus CDP-4,6-dideoxy-4-aminogalactose). In terms of medical applications, E₁ is responsible for making the progenitor to at least four of the seven naturally occurring 3,6-dideoxyhexoses, which in turn confer various pathogenic capabilities to harboring Gram-negative bacteria. The E₁ crystal structures reported herein provide a foundation for the design of inhibitors for the biosynthesis of 3,6-dideoxyhexoses in Gram-negative bacteria.

Supplementary Material

Refer to Web version on PubMed Central for supplementary material.

Acknowledgments

Portions of this research were carried out at the Stanford Synchrotron Radiation Laboratory, a national user facility operated by Stanford University on behalf of the U.S. Department of Energy, Office of Basic Energy Sciences. The SSRL Structural Molecular Biology Program is supported by the Department of Energy, Office of Biological and Environmental Research, and by the National Institutes of Health, National Center for Research Resources, Biomedical Technology Program, and the National Institute of General Medical Sciences. Portions of this research were carried out at the Advanced Light Source, which is supported by the Director, Office of Science, Office of Basic Energy Sciences, of the U.S. Department of Energy under Contract No. DE-AC02-05CH11231. We would additionally like to acknowledge Danny Nam Ho for assistance with figure graphics.

Abbreviations

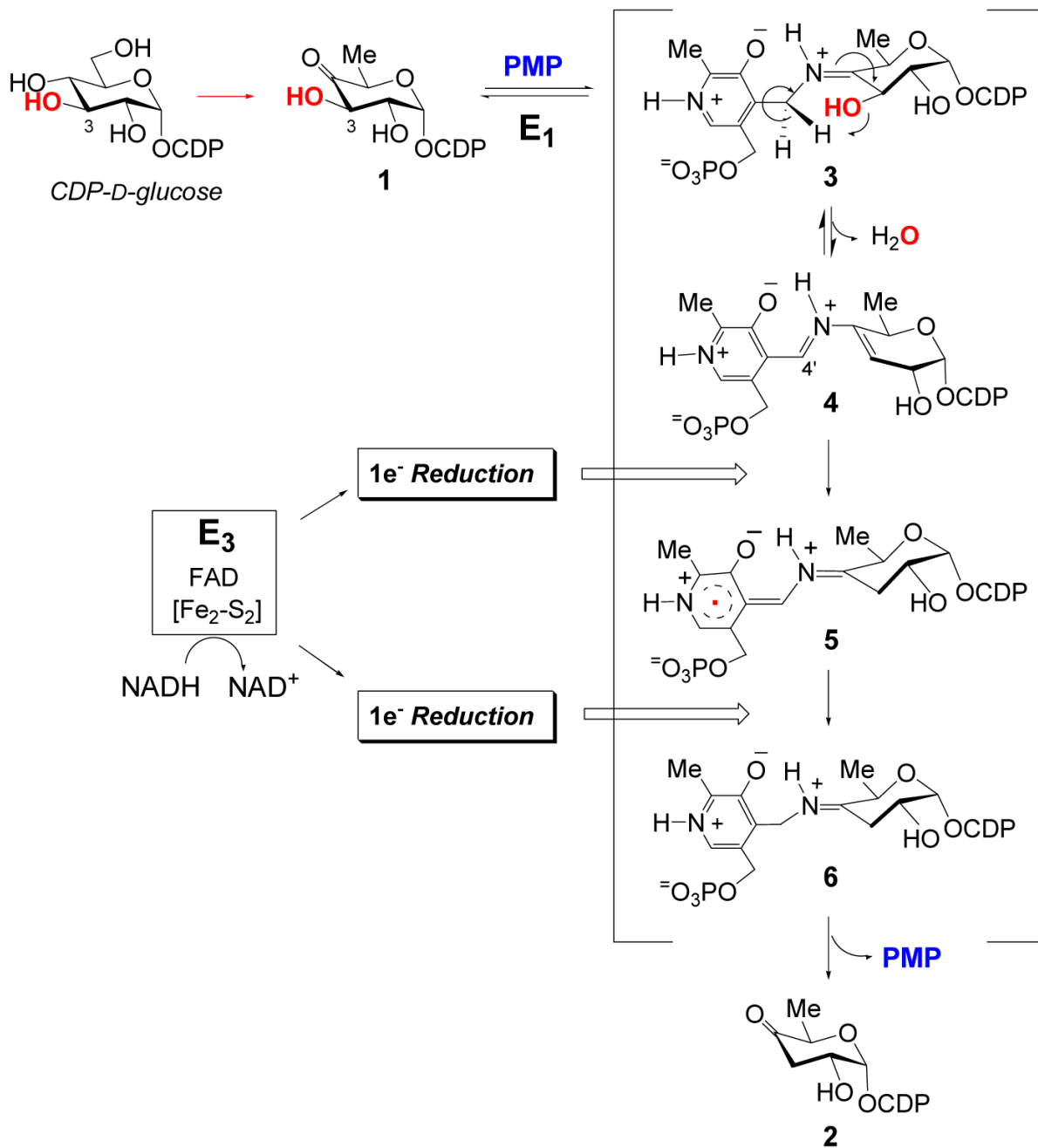
PLP	pyridoxal 5'-phosphate
PMP	pyridoxamine 5'-phosphate
AAT	aspartate aminotransferase
LPS	lipopolysaccharide
NADH	nicotinamide adenine dinucleotide
RMSD	root mean squared deviation
CDP	cytidine diphosphate

ESI-MS	electrospray ionization mass spectrometry
IPTG	isopropyl D-thiogalactoside
DTT	dithiothreitol
LB	Luria-Burtani
DEAE	diethylaminoethyl
SDS-PAGE	sodium dodecyl sulfate polyacrylamide gel electrophoresis
HPLC	high performance liquid chromatography
α-KG	alpha ketoglutarate
PDB	protein data bank

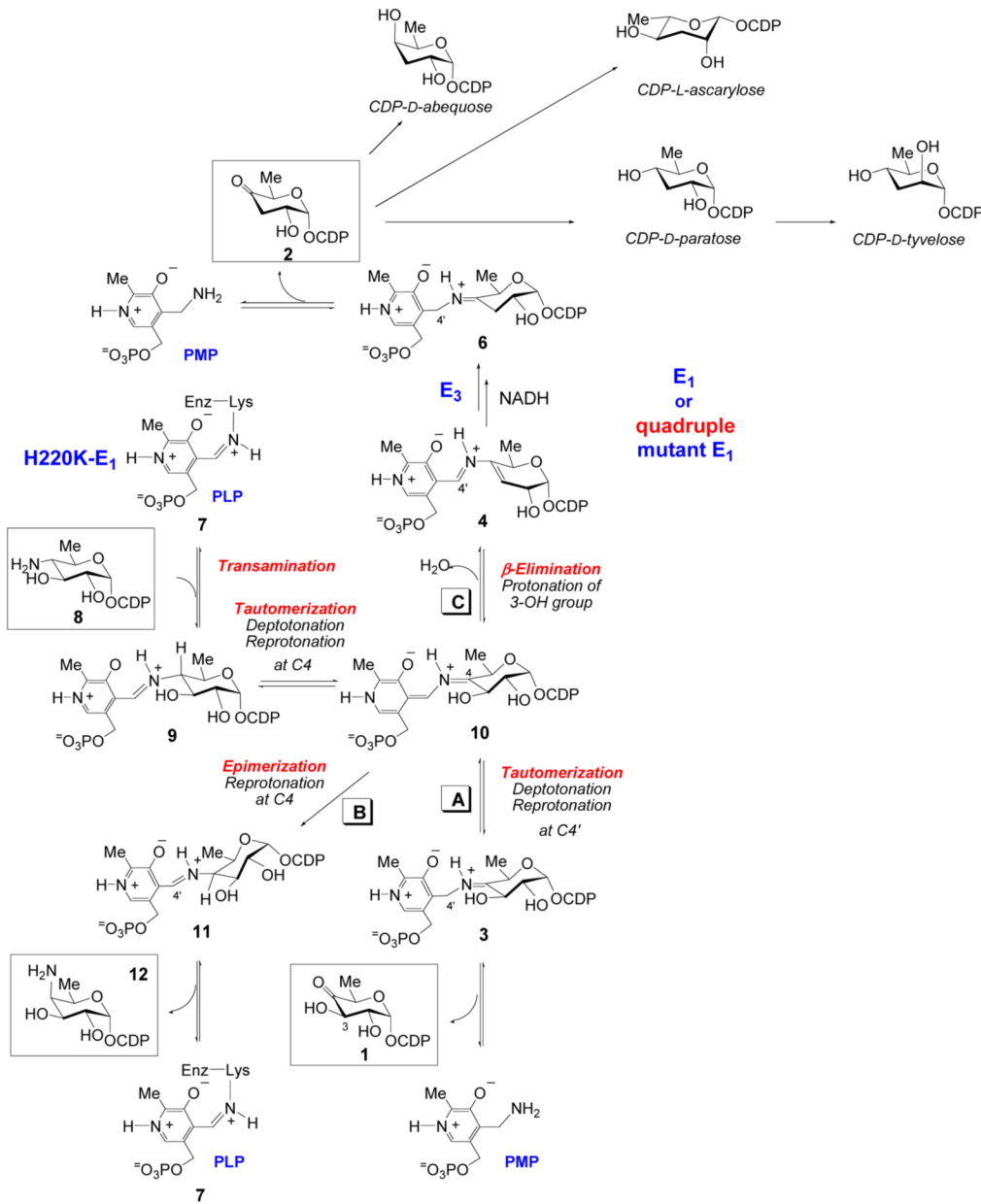
References

1. Dolphin, D.; Poulson, R.; Agramovic, O. Vitamin B6 pyridoxal phosphate chemical, biochemical, and medical aspects. Vol. I. Wiley; 1986.
2. Eliot AC, Krisch JF. Pyridoxal phosphate enzymes: mechanistic, structural, and evolutionary considerations. *Annu Rev Biochem* 2004;73:383–415. [PubMed: 15189147]
3. Wu F, Grossenbacher D, Gehring H. New transition state-based inhibitor for human ornithine decarboxylase inhibits growth of tumor cells. *Mol Cancer Ther* 2007;6:1831–1839. [PubMed: 17575112]
4. Schnell R, Oehlmann W, Singh M, Schneider G. Structural insights into catalysis and inhibition of O-acetylserine sulfhydrylase from *Mycobacterium tuberculosis*: crystal structures of the enzyme {alpha}-aminoacrylate intermediate and an enzyme-inhibitor complex. *J Biol Chem* 2007;282:23473–23481. [PubMed: 17567578]
5. Amadasi A, Bertoldi M, Contestabile R, Bettati S, Cellini B, Luigi di Salvo M, Borri-Voltattorni C, Bossa F, Mozzarelli A. Pyridoxal 5'-phosphate enzymes as targets for therapeutic agents. *Curr Med Chem* 2007;14:1291–1324. [PubMed: 17504214]
6. Liu, H-w; Thorson, JS. Pathways and mechanisms in the biogenesis of novel deoxy sugars by bacteria. *Annu Rev Microbiol* 1994;48:223–256. [PubMed: 7826006]
7. Lindberg B. Components of bacterial polysaccharides. *Adv Carbohydr Chem Biochem* 1990;48:279–318.
8. He, XH-w. Formation of unusual sugars: mechanistic studies and biosynthetic applications. *Annu Rev Biochem* 2002;71:701–754. [PubMed: 12045109]
9. Jansonius JN. Structure, evolution and action of vitamin B6-dependent enzymes. *Curr Opin Struc Biol* 1998;8:759–769.
10. Christen P, Mehta PK. From cofactor to enzymes. the molecular evolution of pyridoxal-5'-phosphate-dependent enzymes. *Chem Rec* 2001;1:437–437.
11. Schneider G, Kack H, Lindqvist Y. The manifold of vitamin B6 dependent enzymes. *Structure* 2000;8:R1–R6. [PubMed: 10673430]
12. Thorson JS, Stanley FL, Liu H-w. Biosynthesis of 3,6-dideoxyhexoses: new mechanistic reflections upon 2,6-dideoxy, 4,6-dideoxy, and amino sugar construction. *J Am Chem Soc* 1993;115:6993–6994.
13. Eads JCB, Scapin G, Yu T-W, Floss HG. Crystal structure of 3-amino-5-hydroxybenzoic acid (AHBA) synthase. *Biochemistry* 1999;38:9840–9849. [PubMed: 10433690]
14. Thorson JS, Liu H-w. Characterization of the first PMP dependent iron-sulfur containing enzyme which is essential for the biosynthesis of 3,6-dideoxyhexoses. *J Am Chem Soc* 1993;115:7539–7540.
15. Agnihotri G, Liu Y-n, Paschal BM, Liu H-w. Identification of an unusual [2Fe-2S]-binding motif in the CDP-6-deoxy-D-glycero-L-threo-4-hexulose-3-dehydratase from *Yersinia pseudotuberculosis*: implication for C-3 deoxygenation in the biosynthesis of 3,6-dideoxyhexoses. *Biochemistry* 2004;43:14265–14274. [PubMed: 15518577]

16. Lei Y, Ploux O, Liu H-w. Mechanistic studies of CDP-6-deoxy-D-glycero-L-threo-4-hexulose-3-dehydratase: identification of His220 as the active-site base by chemical modification and site-directed mutagenesis. *Biochemistry* 1995;34:4643–4654. [PubMed: 7718567]
17. Wu Q, Liu YN, Chen H, Molitor EJ, Liu H-w. A retro-evolution study of CDP-6-deoxy-D-glycero-L-threo-4-hexulose-3-dehydratase (E1) from *Yersinia pseudotuberculosis*: implications for C-3 deoxygenation in the biosynthesis of 3,6-dideoxyhexoses. *Biochemistry* 2007;46:3759–3767. [PubMed: 17323931]
18. Smith P, Lin A, Szu P-H, Liu H-w, Tsai S-C. Biosynthesis of a 3,6-dideoxyhexose: crystallization and x-ray diffraction of CDP-6-deoxy-L-threo-D-glycero-4-hexulose-3-dehydratase (E1) for ascarylose biosynthesis. *Acta Crystallogr F* 2006;62:231–234.
19. Fish WW. Rapid colorimetric micromethod for the quantitation of complexed iron in biological samples. *Methods Enzymol* 1988;158:357–364. [PubMed: 3374387]
20. Otwinowski Z, Minor W. Processing of x-ray diffraction data collected in oscillation mode. *Methods Enzymol* 1997;276:307–326.
21. Brunger AT, Adams PD, Clore GM, DeLano WL, Gros P, Grosse-Kunstleve RW, Jiang JS, Kuszewski J, Nilges M, Pannu NS, Read RJ, Rice LM, Simonson T, Warren GL. Crystallography & NMR system: A new software suite for macromolecular structure determination. *Acta Crystallogr D* 1998;54:905–921. [PubMed: 9757107]
22. Cook PD, Thoden JB, Holden HM. The structure of GDP-4-keto-6-deoxy-D-mannose-3-dehydratase: a unique coenzyme B6-dependent enzyme. *Protein Sci* 2006;15:2093–2106. [PubMed: 16943443]
23. Popovic B, Tang X, Chirgadze DY, Huang F, Blundell TL, Spencer JB. Crystal structures of the PLP- and PMP-bound forms of BtrR, a dual functional aminotransferase involved in butirosin biosynthesis. *Proteins* 2006;65:220–230. [PubMed: 16894611]
24. Badger J, Saunder JM, Adams JM, Antonysamy S, Bain K, Bergseid MG, Buchanan SG, Buchanan MD, Batiyenko Y, Christopher JA, et al. Structural analysis of a set of proteins resulting from a bacterial genomics project. *Proteins* 2005;60:787–796. [PubMed: 16021622]
25. Noland BW, Newman JM, Hendle J, Badger J, Christopher JA, Tresser J, Buchanan MD, Wright TA, Rutter ME, Sanderson WE, Muller-Dieckmann HJ, Gajiwala KS, Buchanan SG. Structural studies of *Salmonella typhimurium* ArnB (PmrH) aminotransferase: a 4-amino-4-deoxy-L-arabinose lipopolysaccharide-modifying enzyme. *Structure* 2002;10:1569–1580. [PubMed: 12429098]
26. Burgie ES, Thoden JB, Holden HM. Molecular architecture of DesV from *Streptomyces venezuelae*: A PLP-dependent transaminase involved in the biosynthesis of the unusual sugar desosamine. *Protein Sci* 2007;16:887–896. [PubMed: 17456741]
27. Schoenhofen IC, Lunin VV, Julien JP, Li Y, Ajamian E, Matte A, Cygler M, Brisson JR, Aubry A, Logan SM, Bhatia S, Wakarchuk WW, Young NM. Structural and functional characterization of PseC, an aminotransferase involved in the biosynthesis of pseudaminic acid, an essential flagellar modification in *Helicobacter pylori*. *J Biol Chem* 2006;281:8907–8916. [PubMed: 16421095]
28. Ford GC, Eichele G, Jansonius JN. Three-dimensional structure of a pyridoxal-phosphate-dependent enzyme, mitochondrial aspartate aminotransferase. *Proc Natl Acad Sci USA* 1980;77:2559–2563. [PubMed: 6930651]
29. Chen XMH, Ploux O, Liu H-w. Biosynthesis of 3,6-dideoxyhexoses: in vivo and in vitro evidence for protein-protein interaction between CDP-6-deoxy-L-threo-D-glycero-4-hexulose-3-dehydratase (E1) and its reductase (E3). *Biochemistry* 1996;35:16412–16420. [PubMed: 8987972]
30. Breazeale SD, Ribeiro AA, Raetz CRH. Origin of lipid A species modified with 4-amino-4deoxy-L-arabinose in polymyxin-resistant mutants of *Escherichia coli*. *J Biol Chem* 2003;278:24731–24739. [PubMed: 12704196]
31. Martinez-Carrión M, Kuczenski R, Tiemeier DC, Peterson DL. The structure and enzyme-coenzyme relationship of supernatant aspartate transaminase after dye sensitized photooxidation. *J Biol Chem* 1970;245:799–805. [PubMed: 4984627]

**Figure 1.**

Starting with CDP-4-keto-6-deoxy-D-glucose (**1**), the E_1 dehydrase catalyzes a PMP-dependent dehydration initiated by the formation of the external aldimine **3**, followed by β -elimination of the 3-OH group to give the quinonoid intermediate **4**, and then reduction by both E_3 and E_1 involving electron relay through FAD and [2Fe-2S] clusters to produce the product CDP-4-keto-3,6-dideoxy-D-glucose (**2**). This product is a common intermediate in the biosynthesis of 3,6-dideoxysugars, such as abequose, paratose, ascarylose and tyvelose, that are important for Gram-negative bacterium pathogenesis.

**Figure 2.**

The versatility of reactions catalyzed by E_1 and its mutants, in addition to representative 3,6-dideoxyhexoses produced from subsequent biosynthetic steps.

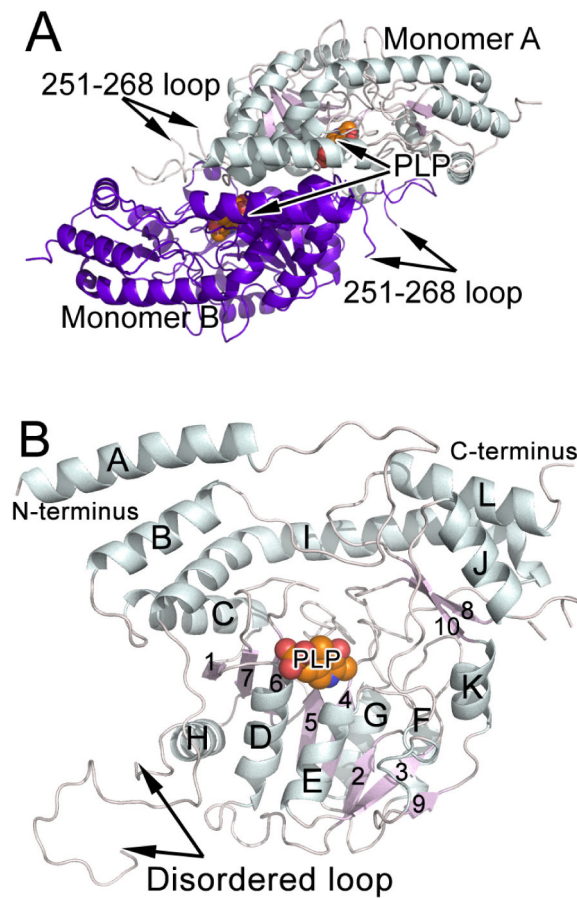
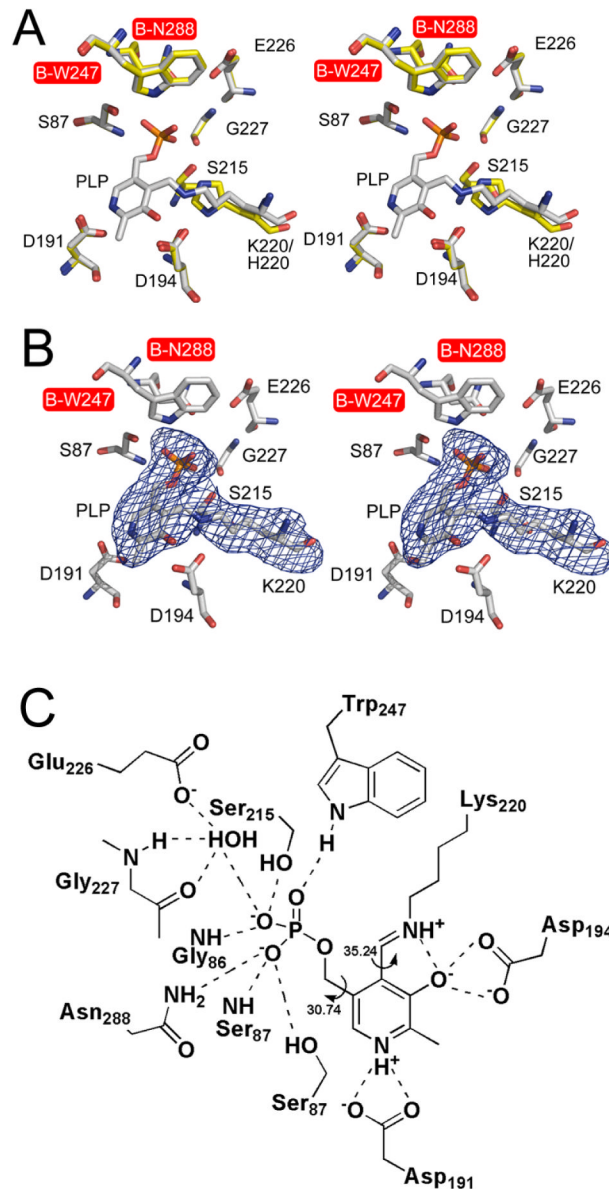
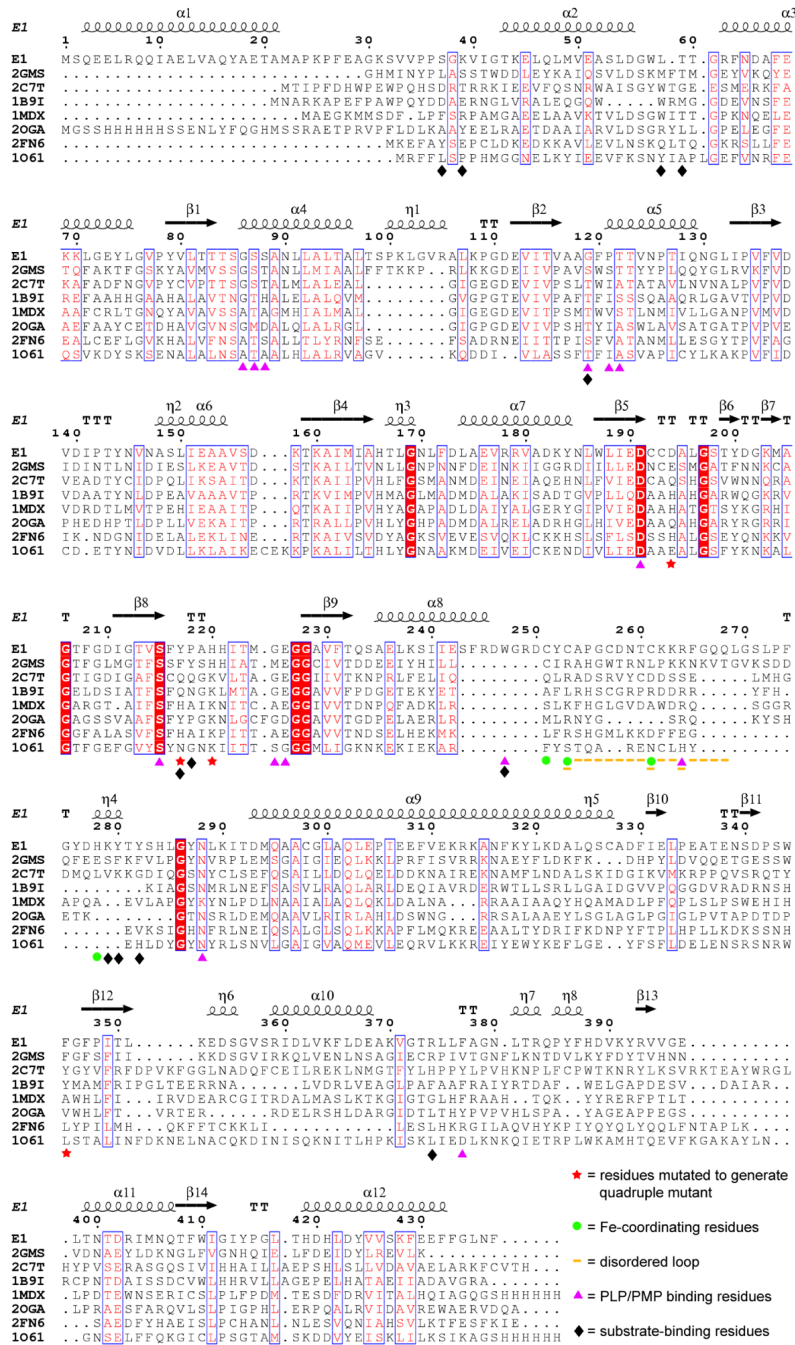


Figure 3.

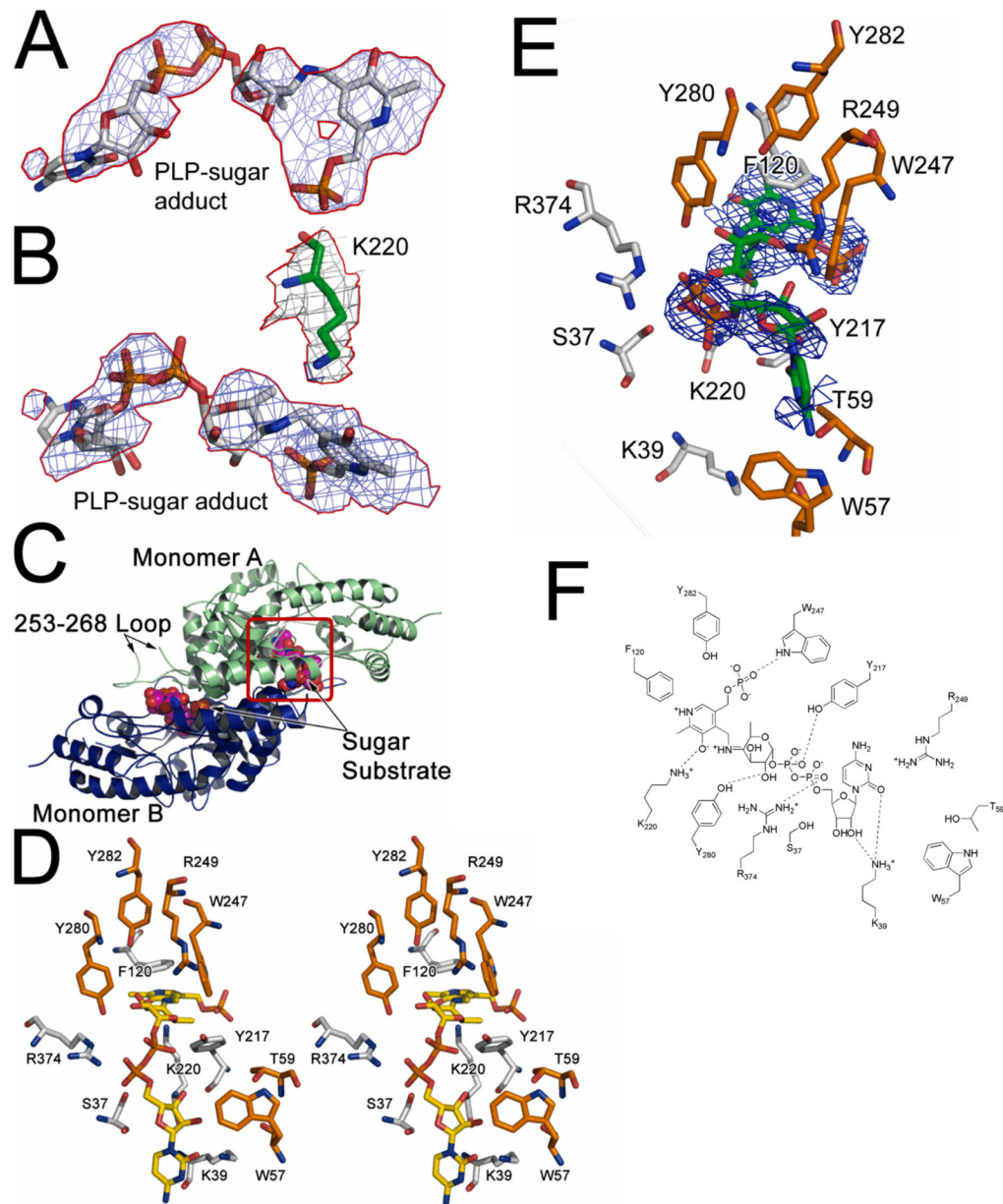
(A) The overall topology of dimeric H220K-E₁, including the cofactor binding site and the putative [2Fe-2S]-binding loop. (B) One H220K-E₁ monomer labeled with all secondary structure elements. The cofactor PLP is shown in spheres.

**Figure 4.**

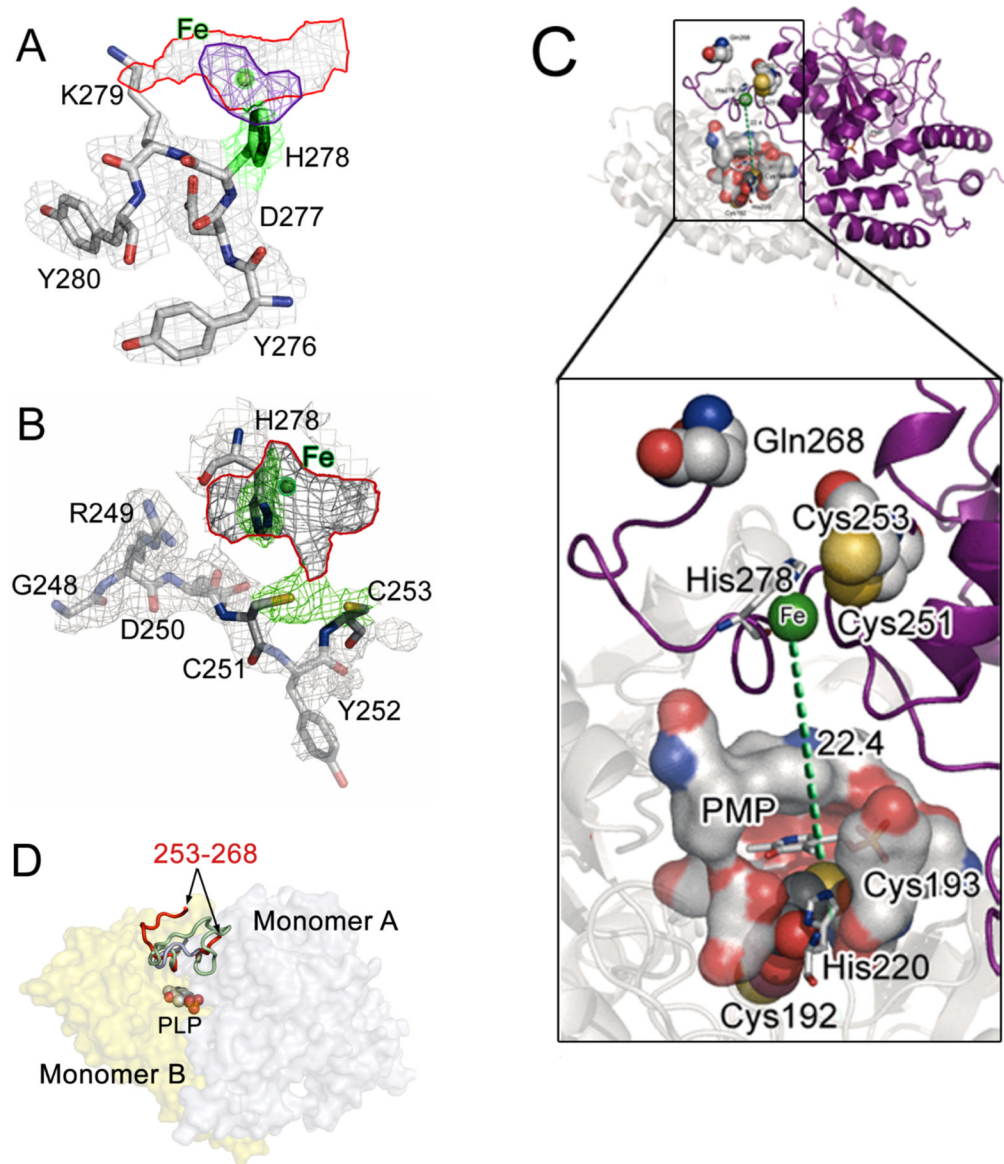
(A) Overlay of wild type and H220K residues in the E₁ active site showing the highly similar architecture. (B) Well-defined PLP/internal lysine aldimine electron density (Fo-Fc omit map, contoured at 3 sigma). (C) Scheme of residues in the wild type E₁ active-site.

**Figure 5.**

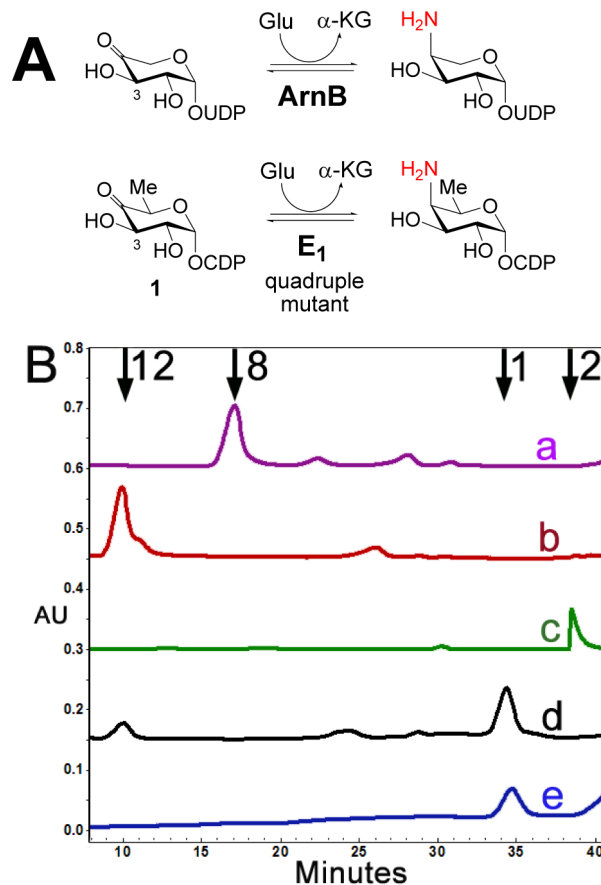
Sequence alignment of E₁ with homologous enzymes. All homologous sequences, identified by their PDB IDs, are aminotransferases (2C7T, 1MDX, 2OGA, 2FN6, 1O6I) or dehydrases (2GMS, 1B9I). Symbols are used to highlight notable structural features of E₁ discussed in the text, where red stars = residues mutated in order to observe aminotransferase activity; green circles = iron binding residues; pink triangles = PLP/PMP-binding residues; orange dashes = disordered loop residues; black diamonds = substrate binding residues.

**Figure 6.**

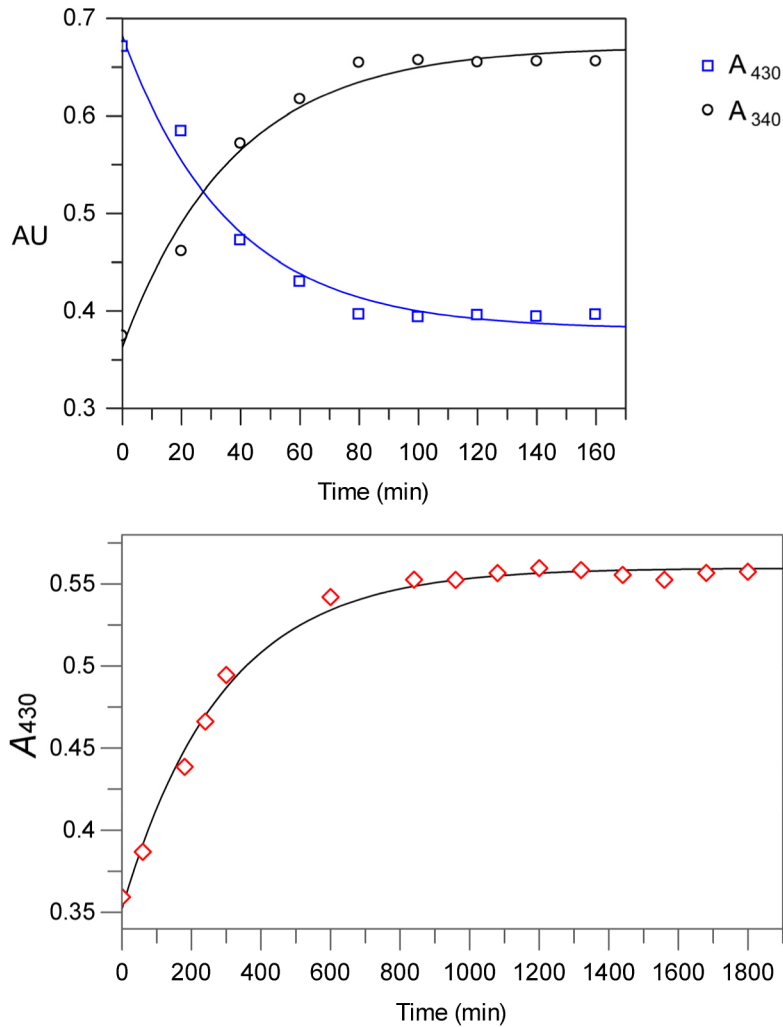
(A) & (B) Two views of the aminosugar-bound structure (CDP-4,6-dideoxy-4-amino-D-glucose **8**) omit map (Fo-Fc, contoured at 3.0 sigma), showing partially defined density of CDP-sugar, and well-defined density of PLP. Note the density between sugar and CDP is broken, but the density of PLP and CDP orients the sugar moiety to the position shown in (A) and (B), which is also consistent with docking simulation of sugar-CDP into E₁. (C) Overall view of the docked sugar substrate **8** in E₁ dimer shows that the bound sugar extends from the coenzyme binding pocket towards the protein surface. (D) Stereo image of docked full substrate (CDP-4,6-dideoxy-4-amino-D-glucose **8**). (E) Similar perspective as D, with the omit map density around external aldimine. (F) Scheme of protein contacts with substrate based upon docking result.

**Figure 7.**

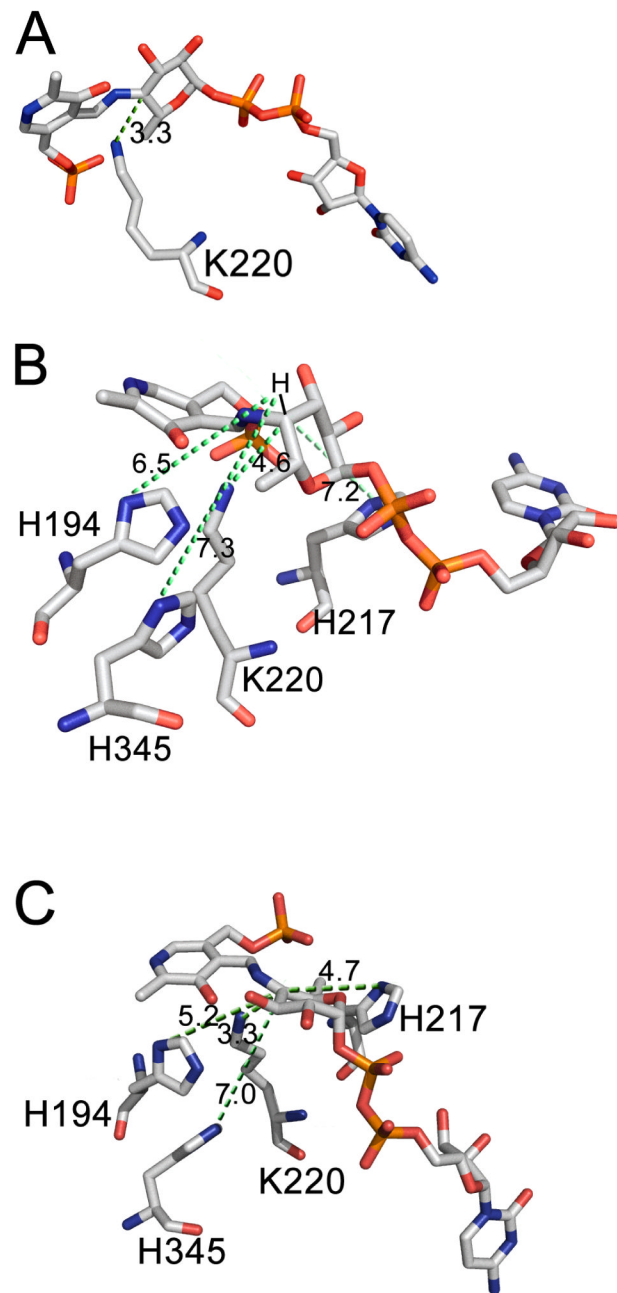
(A) The anomalous iron peak coordinate (green sphere), and electron density calculated with the MAD data (purple, contoured at 5 sigma) lies near the 253-268 loop region. (A) & (B) The omit map in gray density and highlighted green for the H278, C251 and C253 side-chains (Fo-Fc omit map contoured at 3 sigma) displays clear density of H278, and additional, less well-defined density stretching from the proposed iron site indicates protein residues (albeit in disorder) in this region (outlined in red). B is an overhead perspective relative to A, where the difference in the residues displayed in each view is for the sake of clarity. (C) The distance of C192 and C193 is 22–30 Å away from the main [Fe-S] coordinating loop. Hence, the fourth ligand is more likely H278. (D) E₁ dimer with superimposition of loops from homologs with order in this region ((2FN6 (blue), 2GMS (green)), and the disordered E₁ loop in red.

**Figure 8.**

(A) The reaction catalyzed by ArnB aminotransferase is essentially the same as the E₁ quadruple mutant. (B) HPLC trace of the reaction mixture after incubation of the E₁ quadruple mutant with L-glutamate and substrate **1**. Traces from the top, (a), the sugar standards **8** and, (b), **12**, followed by (c), E₁E₃ product **2**, the incubation mixture of the quadruple mutant (d), and the control empty plasmid cell extract (e). The quadruple mutant distinctly produced CDP-4,6-dideoxy-4-aminogalactose **12**.

**Figure 9.**

Spectrophotometric assays of the E₁ quadruple mutant to monitor 1st and 2nd half reactions of stepwise amino transfer from L-glutamate → E-PLP → substrate sugar **1**. Top panel displays plot monitoring the 1st half reaction via the disappearance of E-PLP (A_{430}) and the concurrent appearance of E-PMP (A_{340}) over time, as L-glutamic acid transfers its amide nitrogen to E-PLP to generate E-PMP and α -ketoglutarate (individual data points represent the average of three collected at each time point). Bottom panel displays plot following the 2nd half reaction via appearance of E-PLP (A_{430}) in the presence of E-PMP and substrate **1**, where the amino group from PMP is transferred to the substrate to yield product **12**, and to regenerate E-PLP, thus finishing a catalytic cycle (individual data points represent the average of three collected at each time point). Observed rate constants are tabulated in Table 2.

**Figure 10.**

Docking simulations of (A) the PLP-CDP-6-deoxy-4-aminoglucose adduct **9** that shows K220 is in close proximity to the C4 axial position of the sugar substrate; (B) the PLP-CDP-6-deoxy-4-aminogalactose adduct **11** in the quadruple mutant, in which H194 and H194, instead of K220, are the likely acid/base residues; (C) the quinonoid intermediate **10** in the quadruple mutant revealing both H217 and H194 promote equatorial protonation at C4 of **10** to form **11**. Distances are in angstroms.

Table 1Crystallization, data collection and refinement statistics of E₁

	E₁-Wild type	E₁-H220K	E₁-H220K-Substrate
A. Crystallization	0.1 M Hepes, 2% (v/v) PEG 400, 2 M ammonium sulfate, 2% (w/v) benzamidine HCl (pH 7.5)	0.1 M Hepes, 2% (v/v) PEG 400, 2 M ammonium sulfate, 2% (w/v) benzamidine HCl (pH 7.5)	0.1 M Hepes, 2% (v/v) PEG 400, 2 M ammonium sulfate, 2% (w/v) benzamidine HCl (pH 7.5)
B. Crystallographic Data			
Space Group	P3 ₂	P3 ₂	P3 ₂
Cell Dimension (Å)	97.31, 97.31, 142.35 $\alpha=\beta=90^\circ, \gamma=120^\circ$	98.18, 98.18, 140.39 $\alpha=\beta=90^\circ, \gamma=120^\circ$	98.43, 98.43, 139.77 $\alpha=\beta=90^\circ, \gamma=120^\circ$
Resolution (Å)	50.0–2.40	50.0–2.35	50.0–3.05
Mosaicity (deg.)	0.30	0.28	
No. of Observations	435,918	2,069,783	890,792
No. of Unique Reflections	60,161	63,011	28,217
Completeness % (last shell)	100 (100.0)	99.9 (100.0)	97.3 (98.1)
I/σ(I) (last shell)	15 (3.9)	28.3 (3.3)	19.8 (8.2)
Rmerge % (last shell)	11.6 (42.8)	4.5 (44.7)	7.2 (20.1)
C. Refinement			
Resolution (Å)	50.0–2.40	50.0–2.35	50.0–3.05
No. Reflections	55,314	58,574	26,399
No. Protein Atoms	3,301	3,265	3,265
No. Cofactor Atoms	1	15	15 (hypothetically)
No. Ligand Atoms	0	0	32 (hypothetically)
No. Waters	200	241	0
Rfree %	23.1	25.0	25.9
Rcrs %	20.8	21.9	21.5
D. Geometry			
RMS Bonds (Å)	0.007	0.007	0.008
RMS Angles (deg°)	1.32	1.30	1.37
RMS B Main-chain	1.42	1.39	1.30
RMS B Side-chain	2.15	1.89	2.94
Ramachandran Plot (%)			
Most Favored	86.8	86.9	81.5
Favored	12.1	12.1	17.3
Generously Allowed	0.6	0.4	0.7

The Activity of the E1 Quadruple Mutant.

Smith et al.

Page 24

Table 2

Parameter	* E-PLP (A_{430})			* E-PMP (A_{340})			f_E -PLP (A_{430}) 2 nd half rxn		
	Value	Std.Error	Value	Std.Error	Value	Std.Error	Value	Std.Error	
A_{min}^{-1}	-0.3009	0.0093	0.3083	0.0091	0.2073	0.0034			
k_{min}	0.0277	0.0021	0.0266	0.0020	0.0035	0.0001			
C	0.6818	0.0084	0.3635	0.0082	0.3523	0.0033			

Data fit with equation: $y = A(1 - \exp(-kt)) + C$ $y =$ observed signal; $k =$ apparent first order rate constant; $t =$ time* 1st half reaction f_2 2nd half reaction